Boosting mono-axial crystal field in stable high-coordinate Dy(III) single-ion magnets by substitution of phenoxy axial ligand

Ben Zhang,[a] Yang Zhou,[a] Chang Dong,[a] Yi Xiang,[a] Yanbo Shi,[a] Chennan Zhang,[a] Aihua Yuan,[a] Shaojun Zheng,[a]* Zhao-Yang Li,[b]* Yi-Quan Zhang,[c]* Yong Yang[d] and Lei Chen[a]*

[a]School of Environmental and Chemical Engineering, Jiangsu University of Science and Technology, Zhenjiang 212003, PR China.

[b]School of Materials Science and Engineering, Nankai University, Tianjin 300350, PR China

[c]Jiangsu Key Laboratory for NSLSCS, School of Physical Science and Technology, Nanjing Normal University, Nanjing 210023, PR China

[d]College of Mechanical Engineering, Suzhou University of Science and Technology, Suzhou 215009, PR China

Electronic Supplementary Information

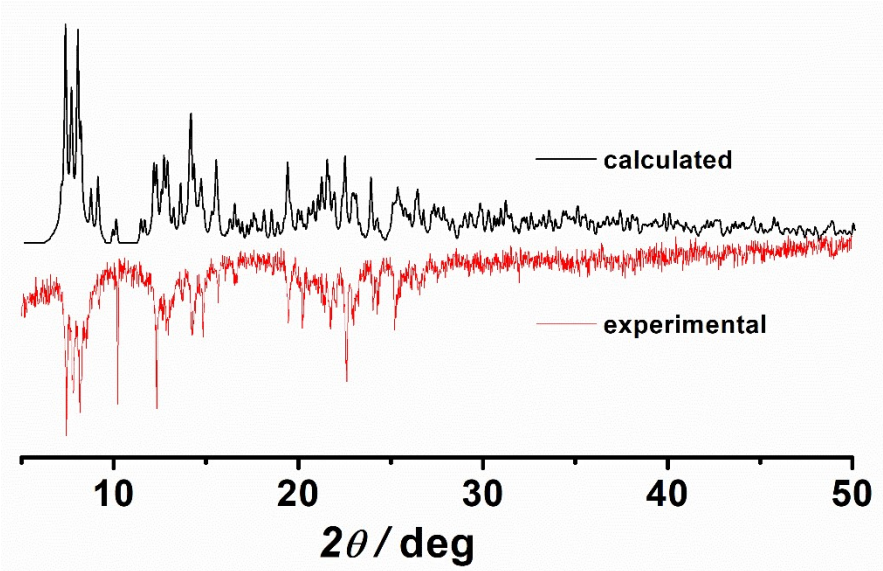

Figure S1. Experimental and simulated X-ray powder diffraction (PXRD) patterns for complex **4**.

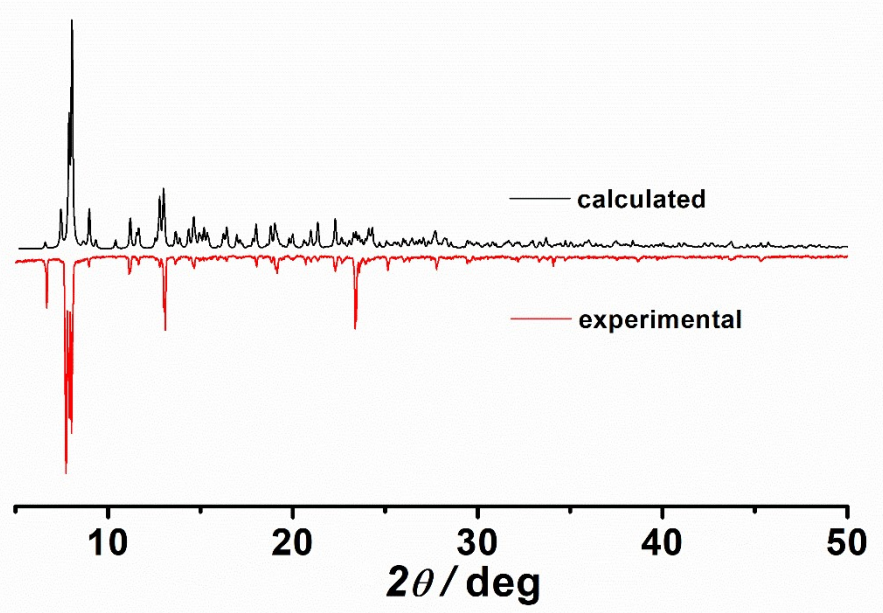

Figure S2. Experimental and simulated X-ray powder diffraction (PXRD) patterns for complex **5**.

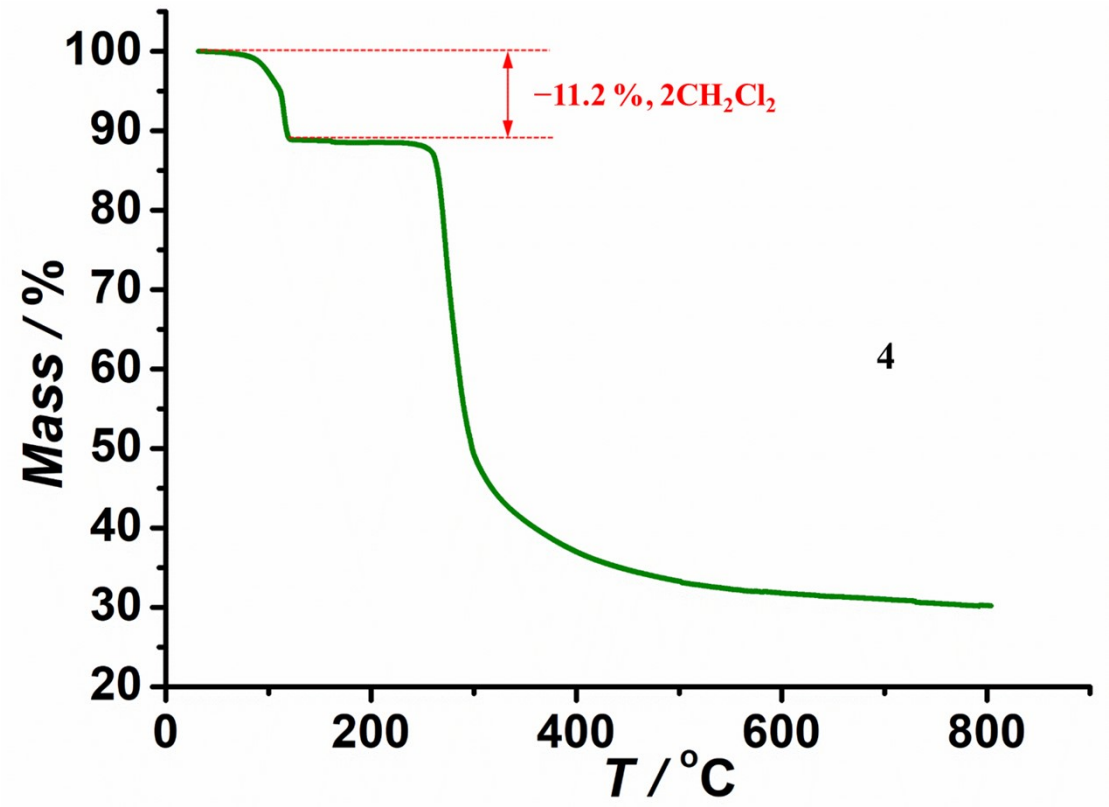

Figure S3. Thermogravimetric analysis of **4**. The red dash lines show the stage of escaping of solvent molecules.

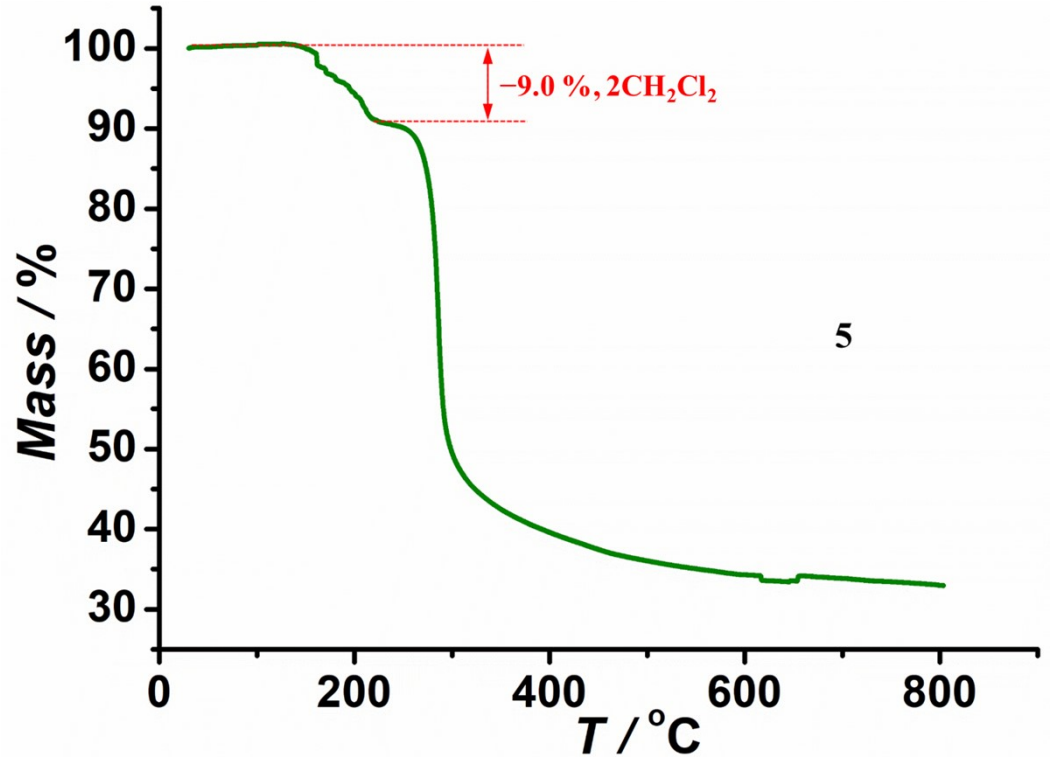

Figure S4. Thermogravimetric analysis of **5**. The red dash lines show the stage of escaping of solvent molecules.

Table S1. Crystal data and structure refinement for **4** and **5**.

	4	**5**
Molecular formula	$C_{89}H_{84}B_2Cl_6DyN_7O_2$	$C_{87.85}H_{81.7}B_2Cl_{1.7}DyN_7O$
CCDC no	2235778	2235779
Formula weight	1680.565	1495.99
Temperature	296(2)	296(2)
Wavelength / Å	0.71073	0.71073
crystal system	Triclinic	Monoclinic
Space group	*P*-1	*P*21/c
a / Å	13.155(3)	20.136(8)
b / Å	14.354(3)	13.581(5)
c / Å	24.759(6)	27.587(11)
α / deg	106.340(13)	90
β / deg	90.908(12)	91.308(10)
γ / deg	115.959(11)	90
V / Å^3	3981.0(17)	7542(5)
Z	2	4
D_{calc}, Mg/m^3	1.402	1.318
μ / mm^{-1}	1.194	1.103
F (000)	1724.7	3083.5
Goodness-of-fit on F^2	1.038	2.050
Final R indices [$I > 2\sigma(I)$][a]	R1 = 0.0334, wR2 = 0.0852	R1 = 0.0297, wR2 = 0.0614
R indices (all data)[a]	R1 = 0.0415, wR2 = 0.0900	R1 = 0.0479, wR2 = 0.0693

[a]$wR_2 = [\Sigma[w(F_o^2–F_c^2)^2]/\Sigma[w(Fo^2)^2]]^{1/2}$, $R_1 = \Sigma||F_o|–|F_c||/\Sigma|F_o|$.

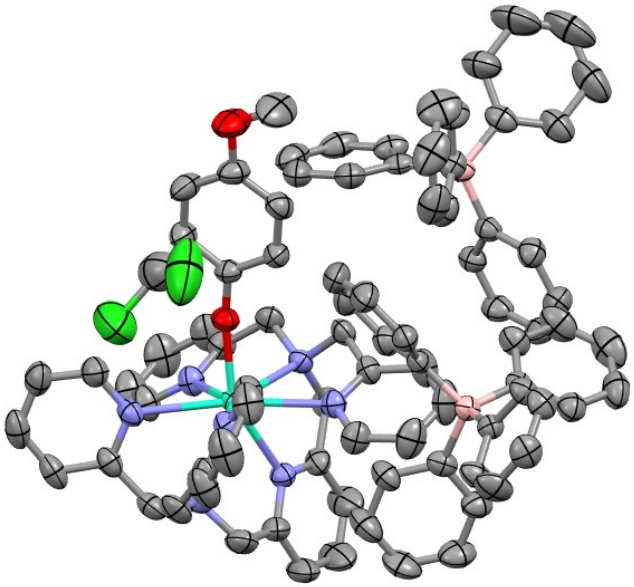

Figure S5. Molecular structure of complex **4**. Thermal ellipsoids are drawn at the 50% probability level. Hydrogen atoms are omitted for clarity.

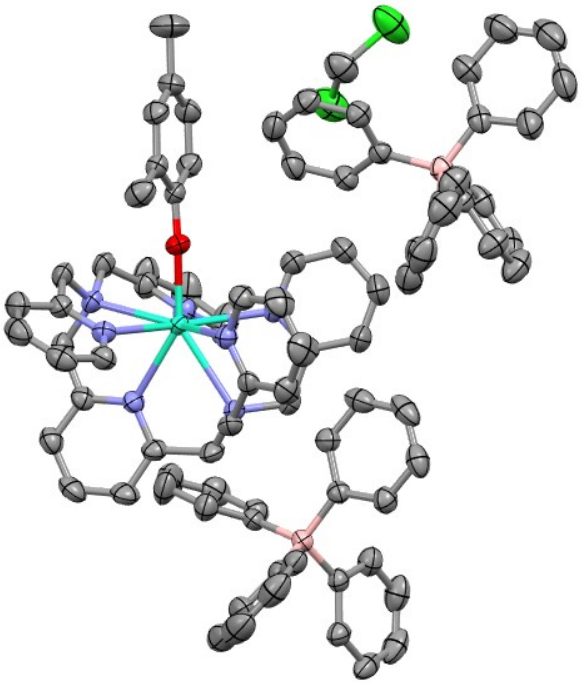

Figure S6. Molecular structure of complex **5**. Thermal ellipsoids are drawn at the 50% probability level. Hydrogen atoms are omitted for clarity.

Table S2. Continuous Shape Measure (CShM) analyses for **4** and **5**. The lowest CShM value is highlighted.

Ideal Polyhedron	**4**	**5**
Octagon (D_{8h})	33.357	30.892
Heptagonal pyramid (C_{7v})	22.085	23.510
Hexagonal bipyramid (D_{6h})	10.966	14.202
Cube (O_h)	8.720	10.879
Square antiprism (D_{4d})	4.389	3.451
Triangular dodecahedron (D_{2d})	**1.990**	**1.774**
Johnson gyrobifastigium (D_{2d})	11.196	12.365
Johnson elongated triangular bipyramid (D_{3h})	25.690	25.385
Biaugmented trigonal prism J50 (C_{2v})	3.914	2.231
Biaugmented trigonal prism (C_{2v})	3.331	1.815
Snub diphenoid (D_{2d})	5.059	3.805
Triakis tetrahedron (T_d)	9.392	11.694
Elongated trigonal bipyramid (D_{3h})	21.364	21.965

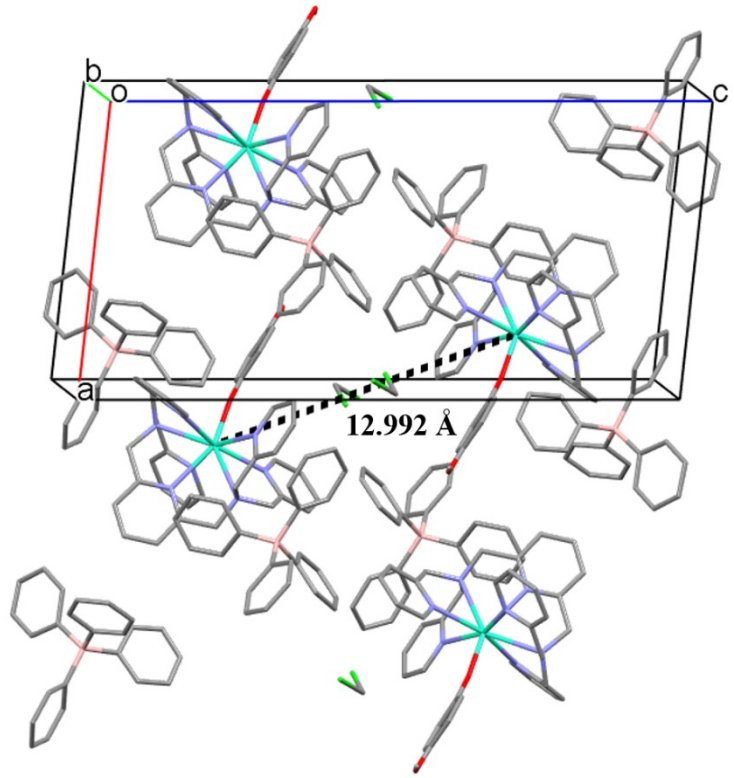

Figure S7. Packing diagram for complex **4**. Hydrogen atoms are omitted for clarity.

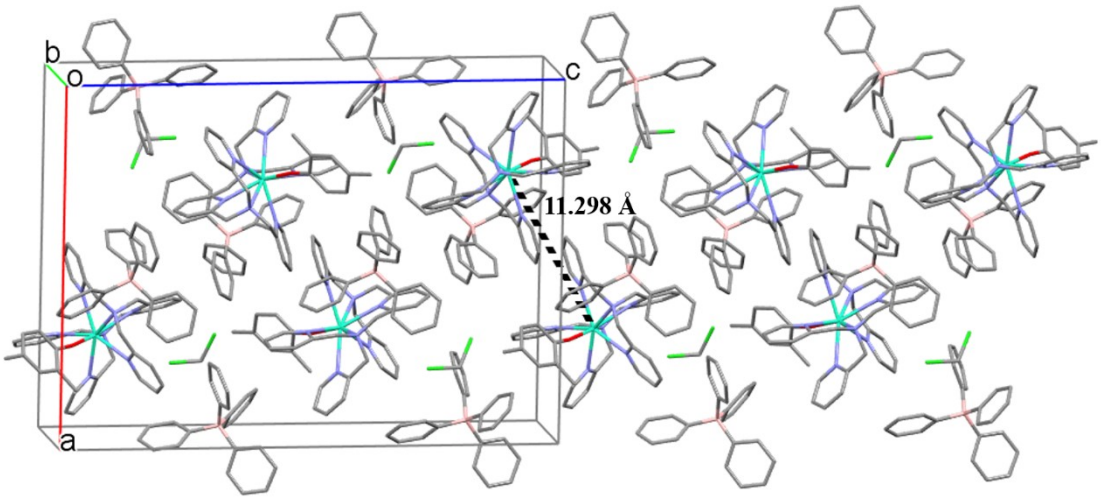

Figure S8. Packing diagram for complex **5**. Hydrogen atoms are omitted for clarity.

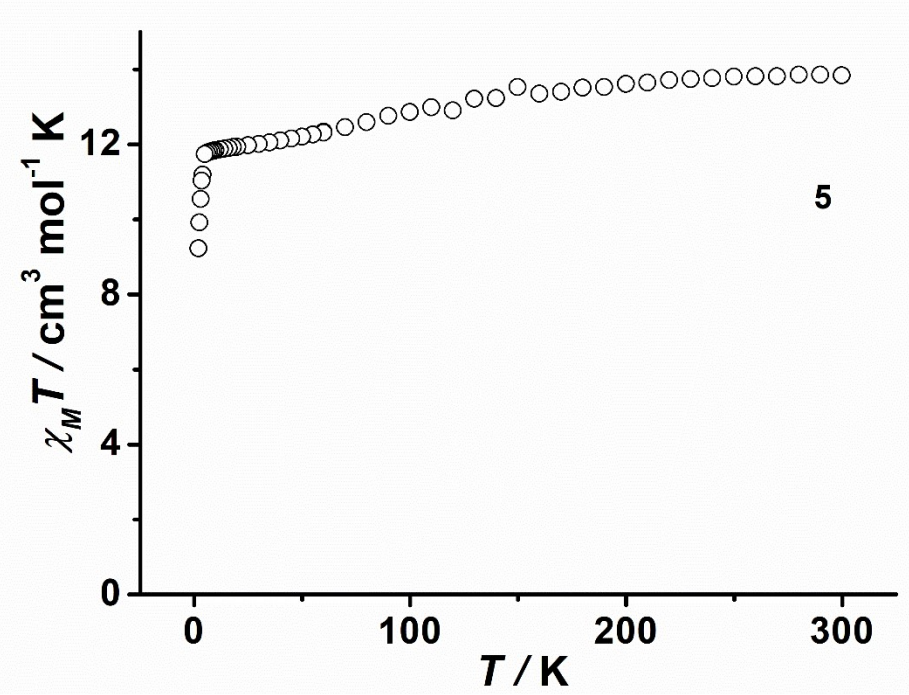

Figure S9. Temperature dependence of the $\chi_M T$ value in an applied magnetic field of 1 kOe for **5**.

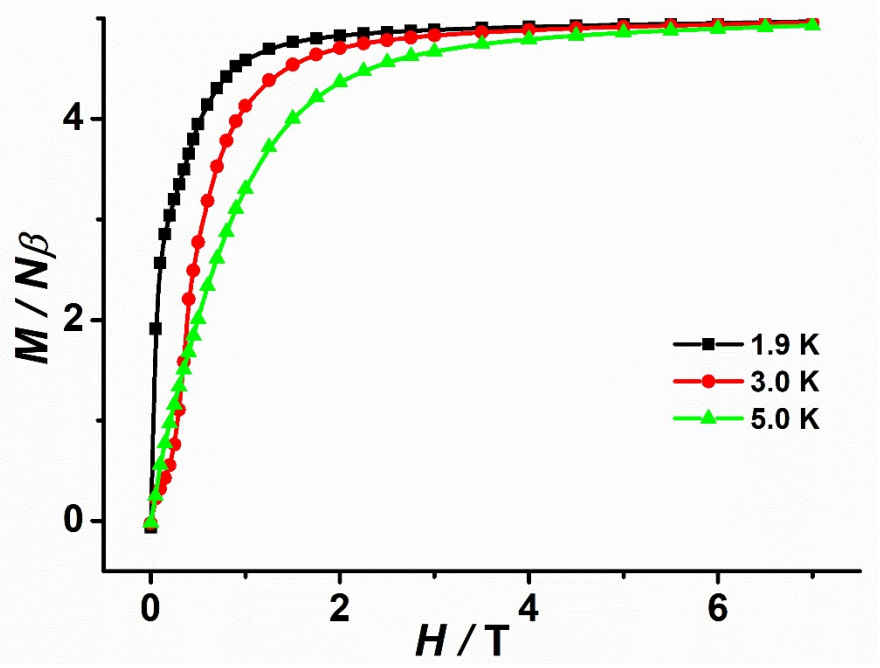

Figure S10. Field dependence of the magnetization at 1.9, 3 and 5 K for **5**.

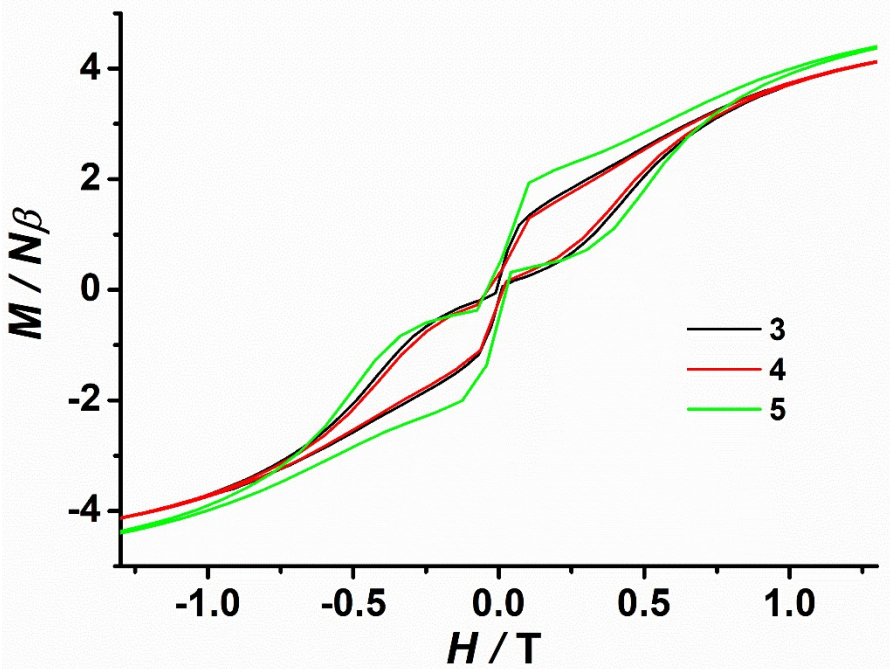

Figure S11. The comparison of magnetic hysteresis loops measurements for **3**, **4** and **5** with an average sweep rate of 0.02 T s^{-1} at 4 K.

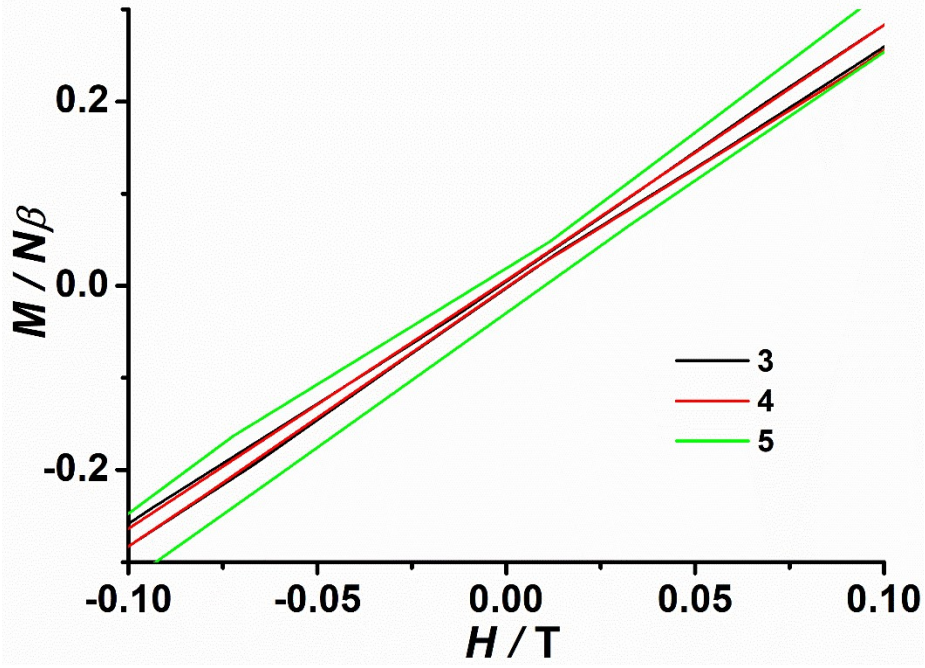

Figure S12. The comparison of magnetic hysteresis loops measurements for **3**, **4** and **5** with an average sweep rate of 0.02 T s^{-1} at 8 K.

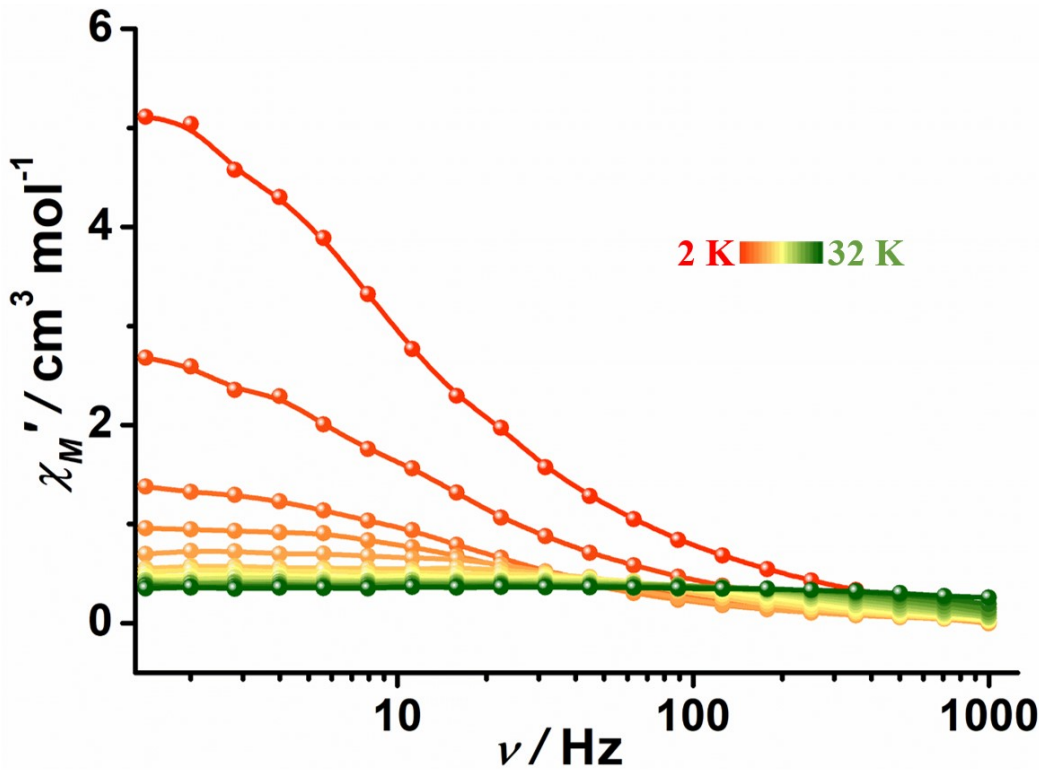

Figure S13. Frequency-dependence of the in-phase susceptibility (χ_M') for **4** under a zero dc field.

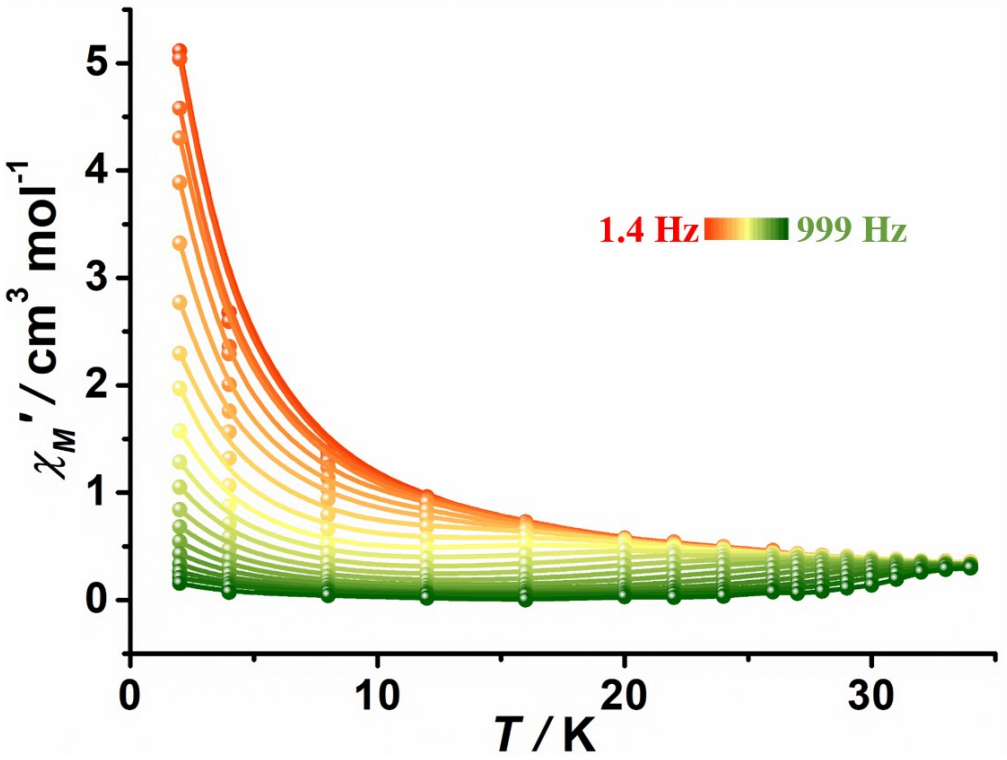

Figure S14. Temperature-dependence of the in-phase susceptibility (χ_M') for **4** under a zero dc field.

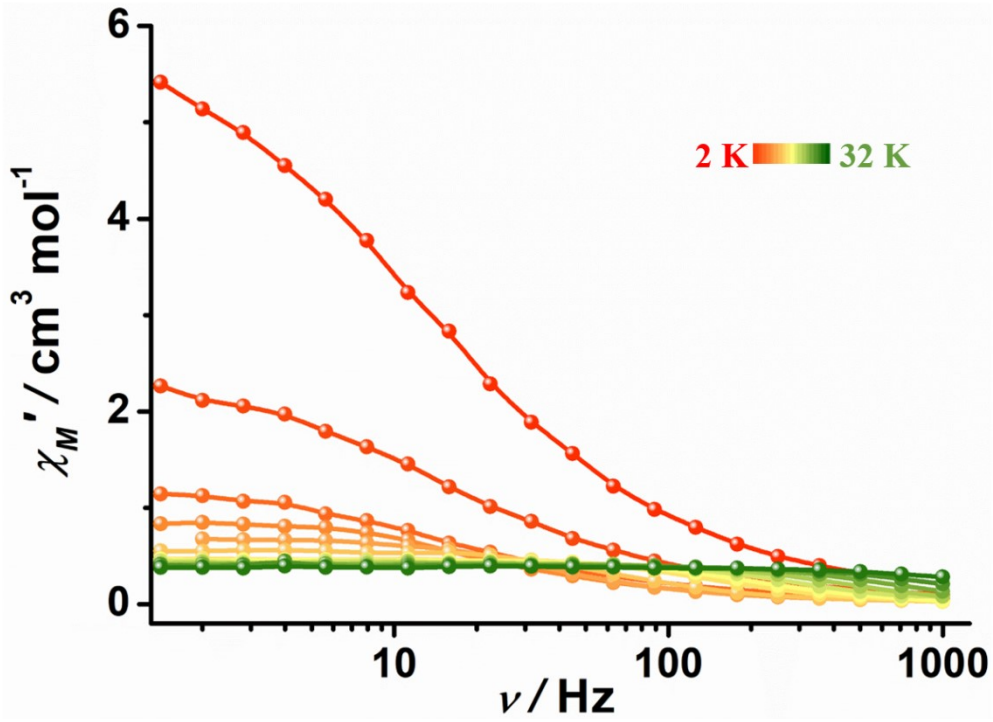

Figure S15. Frequency-dependence of the in-phase susceptibility (χ_M') for **5** under a zero dc field.

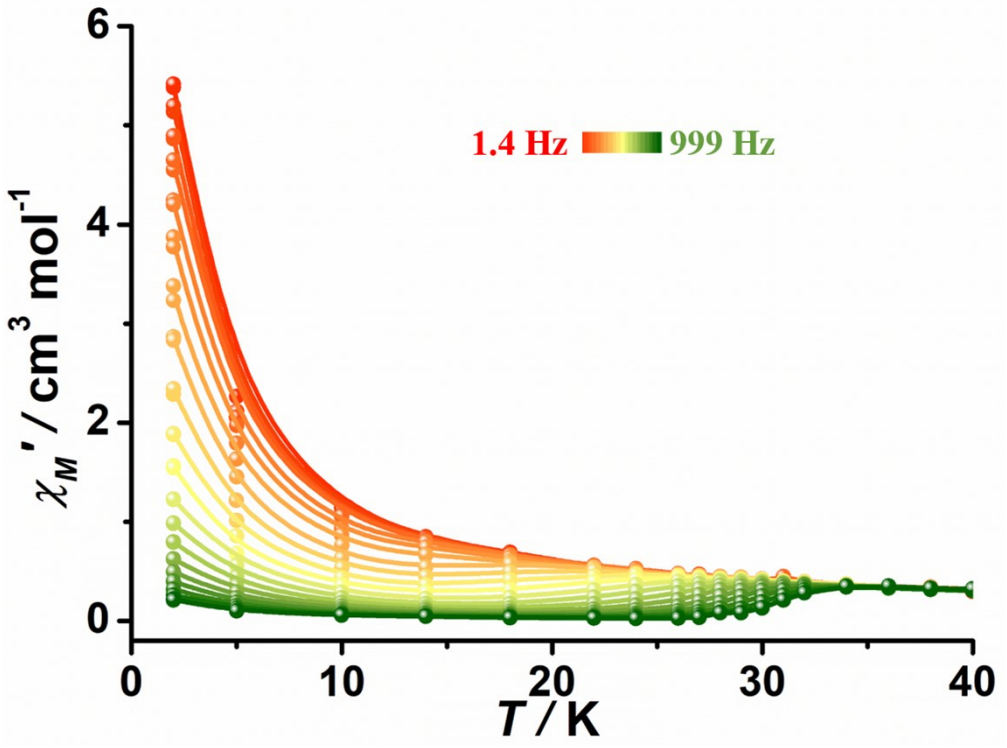

Figure S16. Temperature-dependence of the in-phase susceptibility (χ_M') for **5** under a zero dc field.

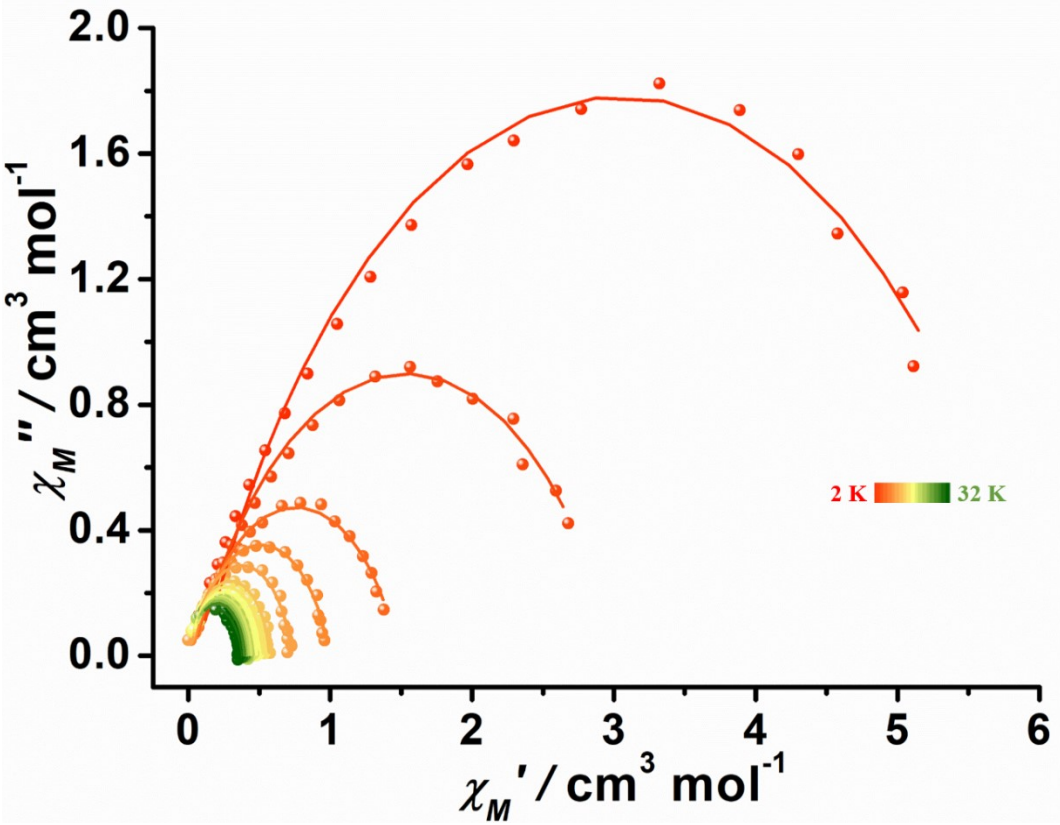

Figure S17. The Cole-Cole plot of **4** in the temperature range of 2−32 K under zero dc field. The solid lines correspond to the best fit to Debye's law.

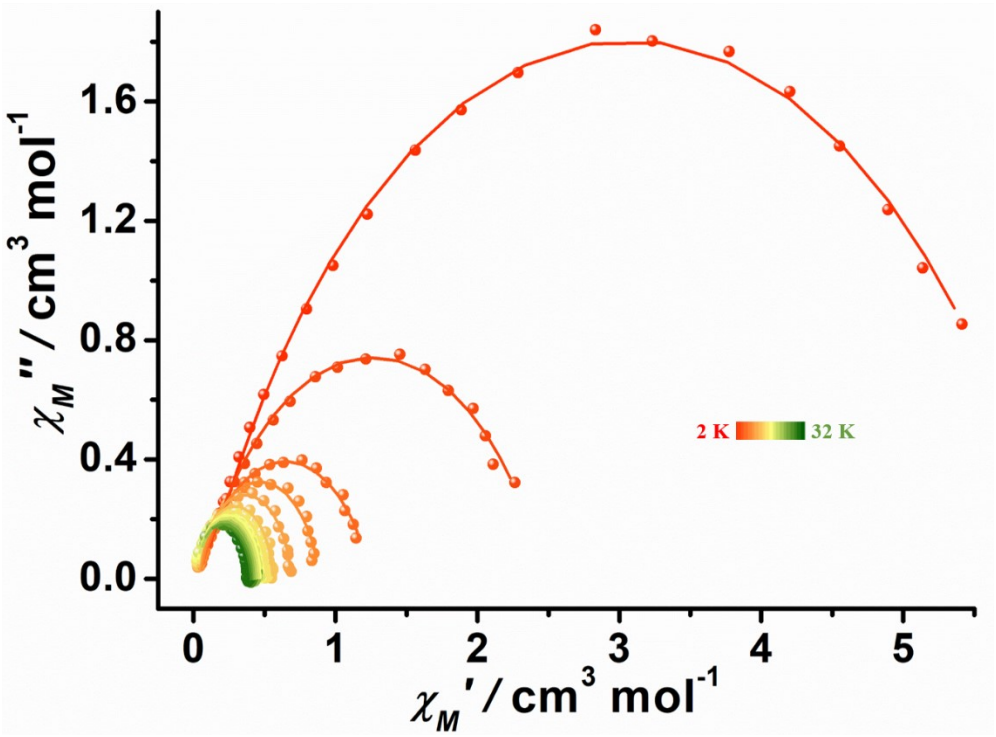

Figure S18. The Cole-Cole plot of **5** in the temperature range of 2−32 K under zero dc field. The solid lines correspond to the best fit to Debye's law.

Table S3. The parameters obtained by fitting the Cole-Cole plot under zero dc field for **4**.

T/K	χ_S	χ_T	τ	a
2	0.0981	5.99659	0.0161	0.31
4	0.0534	3.0111	0.01352	0.30
8	0.03429	1.48054	0.00903	0.26
12	0.0282	0.98873	0.00532	0.19
16	0.02181	0.72493	0.0028	0.12
20	0.02101	0.57149	0.00152	0.09
22	0.0142	0.52652	0.00113	0.09
24	0.01805	0.47953	8.30958×10^{-4}	0.07
26	0.02501	0.44209	5.94822×10^{-4}	0.07
27	0.01716	0.42243	4.7663×10^{-4}	0.06
28	0.02063	0.40669	3.83333×10^{-4}	0.06
29	0.01986	0.3958	2.94392×10^{-4}	0.07
30	0.02769	0.38222	2.27122×10^{-4}	0.07
31	0.03288	0.36915	1.62332×10^{-4}	0.09
32	~0	0.35907	8.9859×10^{-5}	0.14

Table S4. The parameters obtained by fitting the Cole-Cole plot under zero dc field for **5**.

T/K	χ_S	χ_T	τ	a
2	0.08543	6.05644	0.01214	0.31
5	0.05358	2.47372	0.01054	0.30
10	0.03937	1.25193	0.0098	0.27
14	0.04245	0.88993	0.00703	0.16
18	0.0339	0.68937	0.00412	0.09
22	0.02697	0.55864	0.00224	0.05
24	0.02152	0.51482	0.00156	0.05
26	0.02031	0.46914	0.00104	0.02
27	0.01683	0.45628	7.8011×10^{-4}	0.04
28	0.02242	0.43991	5.66185×10^{-4}	0.04
29	0.0172	0.42514	3.87814×10^{-4}	0.04
30	0.0121	0.41192	2.50129×10^{-4}	0.05
31	~0	0.40074	1.49654×10^{-4}	0.08
32	~0	0.38404	9.23521×10^{-5}	0.07

Computational details

Complete-active-space self-consistent field (CASSCF) calculations on mononuclear eight-coordinate complexes **4** and **5** (Figure S19) on the basis of single-crystal X-ray determined geometries have been carried out with OpenMolcas[S1] program package.

The basis sets for all atoms are atomic natural orbitals from the OpenMolcas ANO-RCC library: ANO-RCC-VTZP for Dy^{III}, close N and O; VDZ for distant atoms. The calculations employed the second order Douglas-Kroll-Hess Hamiltonian, where scalar relativistic contractions were taken into account in the basis set and the spin-orbit couplings were handled separately in the restricted active space state interaction (RASSI-SO) procedure.[S2–S3] For complexes **4** and **5**, active electrons in 7 active orbitals include all *f* electrons (CAS(9, 7)) for Dy^{III} in the CASSCF calculations. To exclude all the doubts, we calculated all the roots in the active space. We have mixed the maximum number of spin-free state which was possible with our hardware (all from 21 sextets, 128 from 224 quadruplets, 130 from 490 doublets) for them. SINGLE_ANISO[S4–S6] program was used to obtain the energy levels, ***g*** tensors, magnetic axes, *et al.* based on the above CASSCF/RASSI-SO calculations.

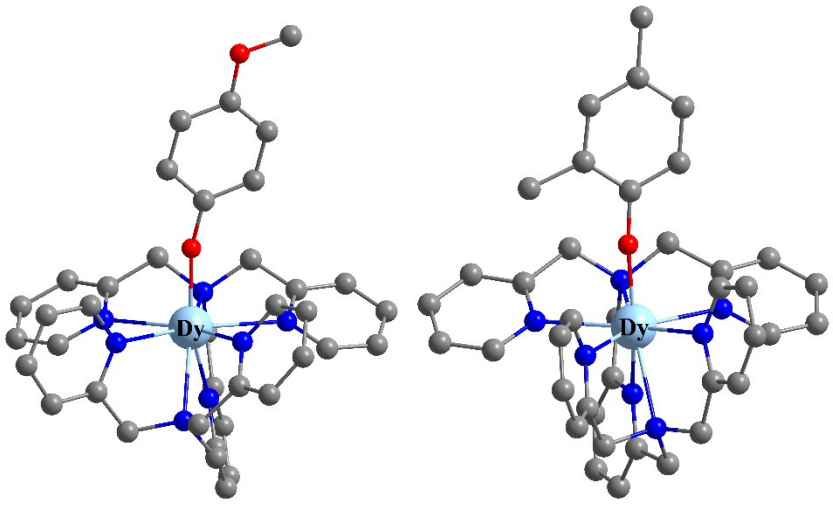

4_Dy **5_Dy**

Figure S19. Calculated molecular structures of complexes **4** and **5**; H atoms are omitted for clarify.

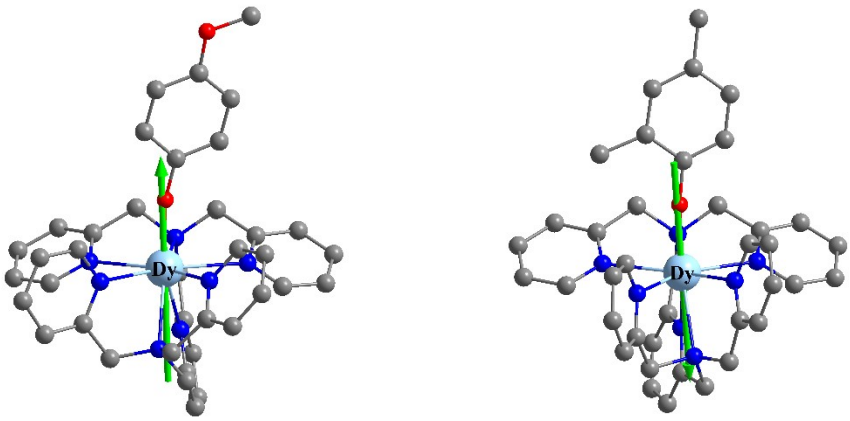

4_Dy **5_Dy**

Figure S20. Calculated orientations of the local main magnetic axes on Dy^{III} ions of complexes **4** and **5** in their ground KDs.

Table S5. Calculated energy levels (cm^{-1}), ***g*** (g_x, g_y, g_z) tensors and predominant m_J values of the lowest eight Kramers doublets (KDs) of complexes **4** and **5** using CASSCF/RASSI-SO with OpenMolcas.

KDs	**4_Dy**			**5_Dy**		
	E/cm^{-1}	***g***	m_J	E/cm^{-1}	***g***	m_J
0	0.0	0.001 0.003 19.849	±15/2	0.0	0.000 0.001 19.857	±15/2
1	304.2	0.147 0.333 17.485	±13/2	316.5	0.138 0.307 16.843	±13/2
2	389.1	2.501 3.595 12.458	-	373.8	2.378 3.444 13.857	-
3	438.6	0.424 2.076 16.647	-	418.7	0.523 5.635 11.573	-
4	480.2	4.128 6.748 10.118	-	465.6	1.517 4.627 10.868	-
5	566.8	0.346 0.871 15.275	-	500.0	1.304 3.595 15.102	-
6	685.7	0.270 1.062 17.521	-	549.1	0.152 0.197 19.225	-
7	719.9	0.294 1.530 17.699	-	638.3	0.061 0.145 19.512	-

Table S6. Wave functions with definite projection of the total moment | m_J > for the lowest eight KDs of complexes **4** and **5** using CASSCF/RASSI-SO with OpenMolcas.

	states	E/cm^{-1}	wave functions
4	KD_0	0.0	99.6%|±15/2>
	KD_1	304.2	67.2%|±13/2>+13.1%|±11/2>+15.0%|±9/2>
	KD_2	389.1	20.7%|±13/2>+16.7%|±11/2>+31.6%|±7/2>+14.8%|±5/2>+7.0%|±9/2>+6.2%|±3/2>
	KD_3	438.6	15.2%|±9/2>+13.8%|±7/2>+34.8%|±5/2>+14.3%|±3/2>+11.4%|±1/2>+8.8%|±11/2>
	KD_4	480.2	22.0%|±11/2>+6.8%|±9/2>+35.6%|±3/2>+24.6%|±1/2>
	KD_5	566.8	15.2%|±11/2>+14.6%|±9/2>+15.3%|±3/2>+45.0%|±1/2>
	KD_6	685.7	11.7%|±11/2>+21.2%|±9/2>+24.7%|±7/2>+18.6%|±5/2>+14.2%|±3/2>+7.1%|±1/2>
	KD_7	719.9	12.4%|±11/2>+19.9%|±9/2>+21.9%|±7/2>+21.8%|±5/2>+13.9%|±3/2>+8.3%|±1/2>
5	KD_0	0.0	99.7%|±15/2>
	KD_1	316.5	82.4%|±13/2>+11.5%|±9/2>
	KD_2	373.8	23.3%|±11/2>+10.6%|±9/2>+36.9%|±7/2>+15.9%|±5/2>+6.9%|±13/2>
	KD_3	418.7	17.1%|±11/2>+18.7%|±9/2>+10.5%|±7/2>+30.0%|±5/2>+15.2%|±3/2>+5.9%|±1/2>
	KD_4	465.6	16.8%|±11/2>+16.1%|±5/2>+40.8%|±3/2>+17.9%|±1/2>
	KD_5	500.0	65.3%|±1/2>+16.3%|±3/2>+8.1%|±9/2>+6.6%|±11/2>
	KD_6	549.1	15.3%|±11/2>+24.5%|±9/2>+21.2%|±7/2>+17.0%|±5/2>+13.9%|±3/2>+5.9%|±1/2>
	KD_7	638.3	15.7%|±11/2>+23.9%|±9/2>+25.9%|±7/2>+19.4%|±5/2>+9.4%|±3/2>

Table S7. Calculated the crystal-field parameters B (k, q) and corresponding weight for compounds **4** and **5** using CASSCF/RASSI-SO with OpenMolcas.

4				**5**			
k	q	B (k, q)	Weight (%)	k	q	B (k, q)	Weight (%)
2	–2	-0.1188×10^{1}	7.92	2	–2	0.1358×10^{1}	11.33
	–1	–0.1735	1.15		–1	–0.1551	1.29
	0	-0.2723×10^{1}	18.17		0	-0.2369×10^{1}	19.76
	1	–0.7232	4.82		1	–0.7409	6.18
	2	-0.2109×10^{1}	14.08		2	–0.4232	3.53
4	–4	0.2190×10^{-2}	2.65	4	–4	-0.1360×10^{-2}	2.05
	–3	0.2455×10^{-2}	2.97		–3	-0.2105×10^{-2}	3.18
	–2	-0.2749×10^{-2}	3.32		–2	0.3553×10^{-2}	5.38
	–1	-0.6904×10^{-3}	0.83		–1	0.9210×10^{-3}	1.39
	0	-0.8654×10^{-2}	10.48		0	-0.8237×10^{-2}	12.47
	1	0.2251×10^{-3}	0.27		1	0.1544×10^{-2}	2.33
	2	-0.3200×10^{-2}	3.87		2	-0.1933×10^{-2}	2.92
	3	0.9054×10^{-3}	1.09		3	0.2587×10^{-3}	0.39
	4	0.1133×10^{-2}	1.37		4	-0.4790×10^{-3}	0.72
6	–6	0.1935×10^{-4}	2.19	6	–6	-0.6564×10^{-5}	0.93
	–5	-0.9483×10^{-5}	1.07		–5	0.7841×10^{-5}	1.11
	–4	0.2505×10^{-4}	2.84		–4	-0.1465×10^{-4}	2.08
	–3	-0.1751×10^{-5}	0.19		–3	-0.9531×10^{-5}	1.35

	–1	0.1742×10^{-4}	1.97		–2	–0.3370×10^{-4}	4.78
	0	0.1858×10^{-4}	2.11		–1	–0.6351×10^{-5}	0.90
	1	–0.2094×10^{-4}	2.37		0	–0.2583×10^{-4}	3.66
	2	0.2909×10^{-4}	3.30		1	0.1181×10^{-4}	1.67
	3	0.3909×10^{-4}	4.44		2	0.1513×10^{-4}	2.14
	4	0.7423×10^{-5}	0.84		3	0.8450×10^{-5}	1.20
	5	0.7272×10^{-5}	0.82		4	–0.1231×10^{-4}	1.74
	6	0.2502×10^{-5}	0.28		5	0.6831×10^{-5}	0.97
		–0.2098×10^{-4}	2.38		6	–0.1911×10^{-4}	2.71

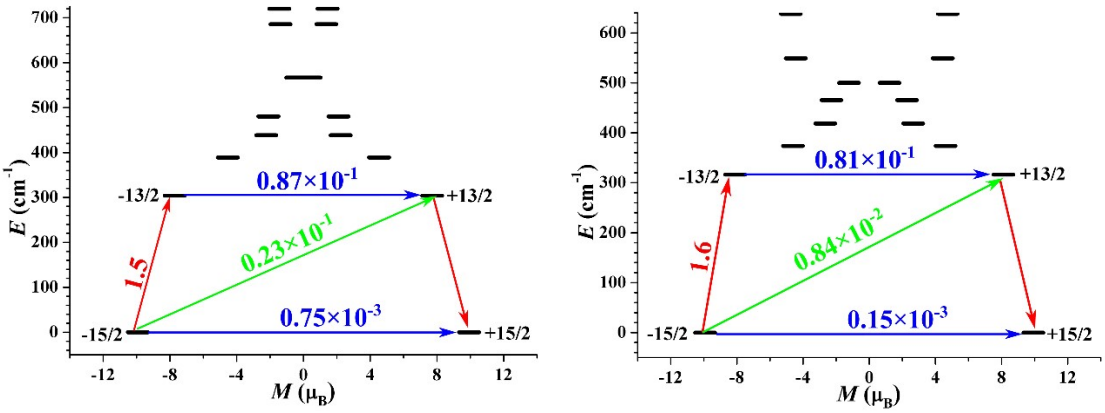

4_Dy **5_Dy**

Figure S21. Magnetization blocking barriers of complexes **4** and **5**. The thick black lines represent the KDs as a function of their magnetic moment along the magnetic axis. The blue lines correspond to diagonal matrix element of the transversal magnetic moment; the green lines represent Orbach relaxation processes. The path shown by the red arrows represents the most probable path for magnetic relaxation in the corresponding compounds. The numbers at each arrow stand for the mean absolute value of the corresponding matrix element of transition magnetic moment.

References

S1 I. F. Galván, M. Vacher, A. Alavi, C. Angeli, F. Aquilante, J. Autschbach, J. J. Bao, S. I. Bokarev, N. A. Bogdanov, R. K. Carlson, L. F. Chibotaru, J. Creutzberg, N. Dattani, M. G. Delcey, S. S. Dong, A. Dreuw, L. Freitag, L. M. Frutos, L. Gagliardi, F. Gendron, A. Giussani, L. González, G. Grell, M. Y. Guo, C. E. Hoyer, M. Johansson, S. Keller, S. Knecht, G. Kovacevic, E. Källman, G. L. Manni, M. Lundberg, Y. J. Ma, S. Mai, J. P. Malhado, P. Å. Malmqvist, P. Marquetand, S. A. Mewes, J. Norell, M. Olivucci, M. Oppel, Q. M. Phung, K. Pierloot, F. Plasser, M. Reiher, A. M. Sand, I. Schapiro, P. Sharma, C. J. Stein, L. K. Sørensen, D. G. Truhlar, M. Ugandi, L. Ungur, A. Valentini, S. Vancoillie, V. Veryazov, O. Weser, T. A. Wesołowski, P.-O. Widmark, S. Wouters, A. Zech, J. P. Zobel and R. Lindh, *J. Chem. Theory Comput.*, 2019, **15**, 5925–5964.

S2 P. Å. Malmqvist, B. O. Roos and B. Schimmelpfennig, *Chem. Phys. Lett.*, 2002, **357***,* 230–240.

S3 B. A. Heß, C. M. Marian, U. Wahlgren and O. Gropen, *Chem. Phys. Lett.*, 1996, **251***,* 365–371.

S4 L. F. Chibotaru, L. Ungur and A. Soncini, *Angew. Chem., Int. Ed*., 2008, **47**, 4126–4129.

S5 L. Ungur, W. Van den Heuvel and L. F. Chibotaru, *New J. Chem.*, 2009, **33**, 1224–1230.

S6 L. F. Chibotaru, L. Ungur, C. Aronica, H. Elmoll, G. Pilet and D. Luneau, *J. Am. Chem. Soc*., 2008, **130**, 12445–12455.